INTERFACE FOCUS

rsfs.royalsocietypublishing.org

Research

Cite this article: Bugli F *et al*. 2018 Curcumin-loaded graphene oxide flakes as an effective antibacterial system against methicillin-resistant *Staphylococcus aureus*. *Interface Focus* **8**: 20170059.
http://dx.doi.org/10.1098/rsfs.2017.0059

Accepted: 31 January 2018

One contribution of 13 to a theme issue 'The biomedical applications of graphene'.

Subject Areas:
biomaterials, nanotechnology, biotechnology

Keywords:
Staphylococcus aureus MRSA, graphene oxide, curcumin, nosocomial infections, targeted therapy

Author for correspondence:
V. Palmieri
e-mail: valentina.palmieri@unicatt.it

†These authors contributed equally to this study.

THE ROYAL SOCIETY PUBLISHING

Curcumin-loaded graphene oxide flakes as an effective antibacterial system against methicillin-resistant *Staphylococcus aureus*

F. Bugli[1,†], M. Cacaci[1,†], V. Palmieri[2,4], R. Di Santo[2], R. Torelli[1], G. Ciasca[2], M. Di Vito[1,5], A. Vitali[3], C. Conti[3], M. Sanguinetti[1], M. De Spirito[2] and M. Papi[2]

[1]Microbiology Institute, Fondazione Policlinico Universitario A. Gemelli, [2]Physics Institute, Fondazione Policlinico Universitario A. Gemelli, and [3]CNR-ICRM, c/o Institute of Biochemistry and Clinical Biochemistry, Catholic University of Sacred Heart, Largo Francesco Vito 1, 00168 Rome, Italy
[4]Institute for Complex Systems, National Research Council (ISC-CNR), Via dei Taurini 19, 00185 Rome, Italy
[5]Dipartimento Scienze Agrarie Università di Bologna Alma Mater Studorium, Bologna, Italy

VP, 0000-0002-6358-9647

Methicillin-resistant *Staphylococcus aureus* (MRSA) is responsible for serious hospital infections worldwide and represents a global public health problem. Curcumin, the major constituent of turmeric, is effective against MRSA but only at cytotoxic concentrations or in combination with antibiotics. The major issue in curcumin-based therapies is the poor solubility of this hydrophobic compound and the cytotoxicity at high doses. In this paper, we describe the efficacy of a composite nanoparticle made of curcumin (CU) and graphene oxide (GO), hereafter GOCU, in MRSA infection treatment. GO is a nanomaterial with a large surface area and high drug-loading capacity. GO has also antibacterial properties due mainly to a mechanical cutting of the bacterial membranes. For this physical mechanism of action, microorganisms are unlikely to develop resistance against this nanomaterial. In this work, we report the capacity of GO to support and stabilize curcumin molecules in a water environment and we demonstrate the efficacy of GOCU against MRSA at a concentration below 2 $\mu g\ ml^{-1}$. Further, GOCU displays low toxicity on fibroblasts cells and avoids haemolysis of red blood cells. Our results indicate that GOCU is a promising nanomaterial against antibiotic-resistant MRSA.

1. Introduction

The increasing administration and use of antibiotics has resulted in the emergence of drug-resistant species: mechanisms such as enzymatic modification, alteration of the target and efflux through pumps are examples of bacterial strategies to develop resistance [1,2].

A public health issue is represented by methicillin-resistant *Staphylococcus aureus* (MRSA), which mainly causes skin and soft tissue infections, with an increasing annual frequency of deaths [3,4]. The rapid spread of antibiotic resistance is posing a serious challenge to its treatment and MRSA has become endemic in many hospitals worldwide [5].

Predisposing factors of bloodstream infections caused by MRSA are skin/soft tissue infections, prosthetic joints or cardiac valves, cardiac electronic devices and central venous catheters and standard empirical choices such as semi-synthetic penicillin, third-generation cephalosporins or carbapenems are inactive against this pathogen [6].

Curcumin, a polyphenolic chemical constituent derived from turmeric, has been shown to significantly decrease the minimal inhibitory concentration (MIC) of the antibiotics currently used against MRSA [7]. Curcumin alone is effective too, but the MIC against MRSA is reported between 125 and 250 $\mu g\ ml^{-1}$ [8]. This concentration is toxic for eukaryotic cells, which display DNA damage if treated with curcumin at concentrations greater than 10 $\mu g\ ml^{-1}$ [8]. In addition to cytotoxicity, curcumin is poorly soluble in water (less than 0.1 $mg\ ml^{-1}$) and

this low bioavailability affects its pharmacological potential [8]. In recent decades, nanotechnology-based delivery systems have been developed for optimizing curcumin therapeutic outcomes as well as minimizing off-target effects [9].

A promising method to deliver curcumin is the use of graphene oxide (GO), a bi-dimensional nanomaterial studied for its excellent chemical and mechanical properties. The ultra-high drug-loading efficiency due to the extremely large surface area of GO has attracted much attention in the drug delivery field [10]. GO has also been studied for its antibacterial properties. Indeed, GO edges can mechanically penetrate membranes and kill bacteria [11–14]. However, GO alone is not active against MRSA at the concentrations tested (MIC $> 60\ \mu g\ ml^{-1}$), but only in composites made of combinations with other antibacterial agents such as silver (silver–GO) or chitosan and silver (chitosan–silver GO) [15,16]. Other proposed methods to kill MRSA are reduced GO–iron oxide nanoparticles and graphene quantum dots. These nanoparticles have light-adsorption properties and after exposure to near-infrared and blue light generate bacterial oxidative stress and death [17,18]. Though promising, these methods are only feasible for local treatment of MRSA infections, due to the low tissue penetrance, especially of blue light. Further, GO efficacy against bacteria is largely dependent on its stability in the environment, and strategies are needed to reduce its cytotoxicity and increase its haemocompatibility [14,19].

Curcumin conjugated to GO has been previously reported as an antitumour drug [20–23] and also as an antimicrobial agent in combination with silver [24]. The use of silver as a bactericidal, however, can cause cumulative toxic effects on patients [25] and induce bacterial resistance [26].

In this paper, we describe the effects of curcumin-conjugated GO (GOCU) and test the antibacterial efficacy of this nanoparticle against MRSA. By using transmission electron microscopy, atomic force microscopy, dynamic light scattering (DLS) and surface zeta potential, we demonstrate efficient curcumin loading on GO sheets with our synthesis method. Furthermore, we analyse antibacterial activity of GOCU against MRSA and compare the GOCU effects to the GO alone, and we consider cytotoxicity on fibroblasts and haemocompatibility. Overall, our data reveal the high antibacterial efficacy and biocompatibility of GOCU and its promising potential to suppress MRSA infections and increase the GO antibacterial effect while improving its biocompatibility.

2. Material and methods

2.1. Sample preparation

GO (Graphenea) in ddH_2O (2 ml) at a concentration of $2\ mg\ ml^{-1}$ was mixed with 2 ml of curcumin (Sigma Aldrich, Milan, Italy) dissolved in ultrapure ethanol at three different concentrations (100, 200 and 300 $\mu g\ ml^{-1}$). Samples were incubated at 70°C for 12 h to let the ethanol completely evaporate. After evaporation, a volume of 2 ml of ddH_2O was added in each sample to have a final concentration of GO of $1\ mg\ ml^{-1}$ and to obtain GOCU-1, GOCU-2 and GOCU-3 samples. Two centrifugation steps (15 min at 14 000 r.p.m.) were used to wash pellets with ddH_2O and remove unbound curcumin and ethanol residuals from the samples. The supernatant was then subjected to UV–Vis analysis to measure the amount of curcumin in excess as reported before [23].

curcumin loading efficiency was determined as follows:

$$\text{curcumin loading efficiency} = \frac{[(W_{\text{initialCur}} - W_{\text{excessCur}})]}{W_{\text{InitialCur}}} \times 100,$$

where $W_{\text{initialCur}}$ is the initial weight of curcumin added and $W_{\text{excessCur}}$ is the weight of curcumin in the supernatant [23].

The final concentration of curcumin and GO was determined by UV/vis adsorption measurements as described in the following. Samples were stored at room temperature (20°C) in dark conditions for further experiments.

2.2. Dynamic light scattering and zeta potential measurements

Size and ζ potential of GO flakes with or without curcumin were assessed by using Zetasizer Nano ZS (Malvern, Herrenberg, Germany). DLS measurements were performed with a 633 nm He–Ne laser operating at an angle of 173°. Solvent-resistant cuvettes (ZEN0040, Malvern, Herrenberg, Germany) were used for experiments with a sample volume of 40 µl. The measurements were performed at a fixed position (4.65 mm) with an automatic attenuator and at a controlled temperature (20°C) as reported previously [27]. For each sample, five measurements were averaged, and the diffusion coefficient D was retrieved through cumulants analysis of autocorrelation functions. The equivalent hydrodynamic radius (Z-Average size) was obtained by the Stokes–Einstein equation. Data analysis was performed by Malvern Zetasizer software. The ζ potential was calculated from the electrophoretic mobility by means of the Henry correction to Smoluchowski's equation [28].

2.3. Adsorption spectra

Experiments were performed with a Cytation 3 Cell Imaging Multi-Mode Reader (Biotek Instruments) using 100 µl of each sample in flat-bottomed 96-well plates (Thermo Fisher Scientific, MA, USA). Absorption spectra were recorded from 230 to 700 nm with steps of 5 nm. Data were analysed with Microsoft Excel software.

2.4. Atomic force microscopy measurements

Samples were prepared as explained elsewhere [29]. Briefly, a 20 µl aliquot of sample was deposited on sterile freshly cleaved mica discs, air-dried and measured with a NanoWizard II atomic force microscope (JPK Instruments AG, Berlin, Germany). The images were acquired using silicon cantilevers with high-aspect-ratio conical silicon tips (CSC37 Mikro-Masch, Tallinn, Estonia) characterized by an end radius of about 10 nm and a half conical angle of 20°. Cantilevers with a nominal spring constant of about $k = 0.4\ N\ m^{-1}$ were calibrated as previously reported [29,30].

2.5. Antibacterial activity of graphene oxide and curcumin-conjugated graphene oxide

MRSA was grown in LB medium at 37°C overnight, then sub-inoculated in fresh LB and harvested in the mid-exponential phase via centrifugation (4000 r.p.m. for 10 min). Cells were washed three times with saline solution (0,9%) to remove residual macromolecules and other LB constituents. The pellets were then suspended in saline solution to obtain cell samples having a McFarland turbidity of 0.5 corresponding to 10^7–$10^8\ CFU\ ml^{-1}$. A 100 µl aliquot of bacterial suspension was mixed with 100 µl of GO/GOCU. Cells were incubated with GO/GOCU for four hours at room temperature. After incubation, colony-forming units (CFUs) were quantified with serial 10-fold microdilutions as reported previously [14].

After interaction with GO or GOCU, 20 µl of each sample was transferred into 180 µl of fresh LB broth, and growth was followed by measuring the optical density (OD) (600 nm) every 15 min with a Cytation 3 Cell Imaging Multi-Mode Reader, at a controlled temperature (37°C) for 24 h. After 24 h, the MIC was evaluated as the lowest concentration that inhibits visible bacterial growth, as reported elsewhere [31].

To determine the minimal bactericidal concentration (MBC) values, the well plates were incubated under identical conditions for 24 h. Then, the bacterial suspension in each well was collected and plated, and CFUs were analysed [16]. MBC was defined as the lowest drug concentration at which 99.9% of the bacteria were killed.

2.6. Transmission electron microscopy

Samples were fixed in glutaraldehyde (2.5%) and imaged after negative staining with uranyl acetate (2%) with a Zeiss Libra 120 Transmission electron microscope (Germany), as reported elsewhere [32].

2.7. Cytotoxicity measurements

The cytotoxic effects of GO and GOCU complexes were studied on a 3T3 fibroblast cell line, using a commercial CellTiter-Blue® cell viability assay (Promega, WI, USA). Unless otherwise specified, all chemicals and reagents used in this section were obtained from Sigma (Milan, Italy). Mouse 3T3 fibroblasts (Swiss albino mouse cell line—Istituto Zooprofilattico, Brescia, Italy) were cultured at 37°C in a humidified environment (CO_2 5%) in DMEM supplemented with 10% fetal calf serum, 500 units ml^{-1} penicillin, 10 mg ml^{-1} streptomycin and 20 mM L-glutamine. In toxicity assays, cells (1×10^4) in basal medium (200 µl) were seeded in individual wells of a 96-well tissue culture plate to a sub-confluent monolayer. Cell synchronization was performed, culturing the cells in a serum-free medium for 24 h. Cellular viability was evaluated after 24 and 48 h upon addition of GO or GOCU solutions for a final GO concentration of 50 µg ml^{-1} for each sample. The fluorescence (560Ex/590Em) of the solution was determined using an automatic microplate reader (Glomax, Promega, WI, USA). The readings were performed after an incubation of 2.5 h at 37°C with the reagent. Each experiment was performed in triplicate.

2.8. Haemolytic activity of graphene oxide and curcumin-conjugated graphene oxide

Human whole blood was obtained by venepuncture of 10 healthy volunteers at the Policlinico Gemelli of Rome in accordance with the institutional bioethics code. Whole blood (1 ml) was diluted and centrifuged at 500*g* for 5 min to isolate red blood cells (RBCs) from serum. To test the haemolytic activity, 0.2 ml of diluted RBC solution was added to 0.8 ml of GO and GOCU and allowed to interact at 37°C for 3 h. RBCs in ddH_2O or in saline buffer were used as positive and negative control, respectively. After incubation, the samples were centrifuged, the supernatant haemoglobin measured spectrophotometrically (540 nm) and the percentage of haemolysis was calculated as reported previously [27].

2.8.1. Oxidative stress measurement

Glutathione (GSH) oxidation by GO and GOCU was measured in acellular conditions using a method described previously [33]. Reduced GSH (0.4 mM) was exposed to GO/GOCU (50 µg ml^{-1}) in a total volume of 10 ml of 50 mM bicarbonate buffer (pH 8.6). Samples were exposed at room temperature for 3 h in the dark. The amount of non-oxidized GSH was quantified spectrophotometrically using Ellman's reagent (5,50-dithiobis(2-nitrobenzoic acid), DTNB), which reacts with thiol groups of GSH. The reaction medium was filtered (0.45 µm), then 900 µl of the filtered reaction mixture was added to 1.57 ml Tris–HCl buffer (pH 8.3) to which 30 µl of 100 mM DTNB was added. The amount of thiol remaining in the reaction medium was quantified by measuring TNB absorbance at 412 nm, using an extinction coefficient of 14 150 M^{-1} cm^{-1}. Samples without GO have been used as negative controls, while diamide (TMAD, Sigma) has been used as the positive control for complete oxidation of GSH [34].

3. Results and discussion

3.1. Characterization of graphene oxide and curcumin-conjugated graphene oxide

In figure 1, the characterization of GO and GOCU-2 materials is reported. From representative TEM images, it is clearly visible how GO sheets have a smooth surface and a smaller size (figure 1*a*) compared to the rougher and larger GOCU-2 sheets (figure 1*b*). Atomic force microscopy (AFM) profiles and images shown in figure 1*c* confirm this evidence with an average sheet height of approximately 0.87 nm for GO compared to approximately 1.65 nm for GOCU-2 (figure 1*d*). The curcumin is uniformly distributed on the GOCU-2 surface that displays an RMS of approximately 0.6 nm compared to approximately 0.2 nm for GO (figure 1*d*). The increase in the thickness and roughness of the GOCU sheets (when compared with the GO alone) is attributed to $\pi-\pi$ attachment of curcumin molecules on the GO surface, as previously demonstrated for curcumin [20] and other aromatic molecules [35], such as ginseng [36], vitamin C [37], melatonin [38] and polyphenols of green tea [39].

Using DLS measurements, the mean hydrodynamic radius (R_H) of bare GO is approximately 540 nm, compared to the approximately 3.4 µm for GOCU-2, indicating that curcumin molecules on the GO surface cause the bridging of multiple sheets. The presence of curcumin shielding the GO surface is demonstrated by the values of zeta potential of approximately −31.4 mV for GO and of approximately −24.6 mV for GOCU-2 (figure 1*d*).

To quantify the amount of curcumin per GO sheet, we used its UV–Vis absorption properties after desorption of curcumin molecules from the GO surfaces in ethanol as previously reported in the literature [23,40]. The curcumin (in ethanol) and GO (in water) adsorption spectra at different concentrations are reported in figure 2. The shape of GO spectra has typical decay due to the particle light scattering without adsorption peaks at wavelengths investigated (figure 2*a*). On the other hand, curcumin shows an absorption peak at 430 nm that has been used for calibration curve tracing and quantification (figure 2*b*). In the insets, the calibration curve and fitting equation obtained from adsorption at 430 nm for GO (figure 2*a*) and curcumin (figure 2*b*) are shown.

Since in the water environment curcumin and thus GOCU fluorescence is quenched [41], to precisely quantify the amount of curcumin bound to GO sheets, we diluted GOCU samples in ultrapure ethanol prior to analysing the intensity peaks at 430 nm [23]. As expected, the amount of curcumin bound to GO is proportional to the initial curcumin concentration. Final curcumin concentrations and loading efficiency in each sample are reported in figure 2*c*.

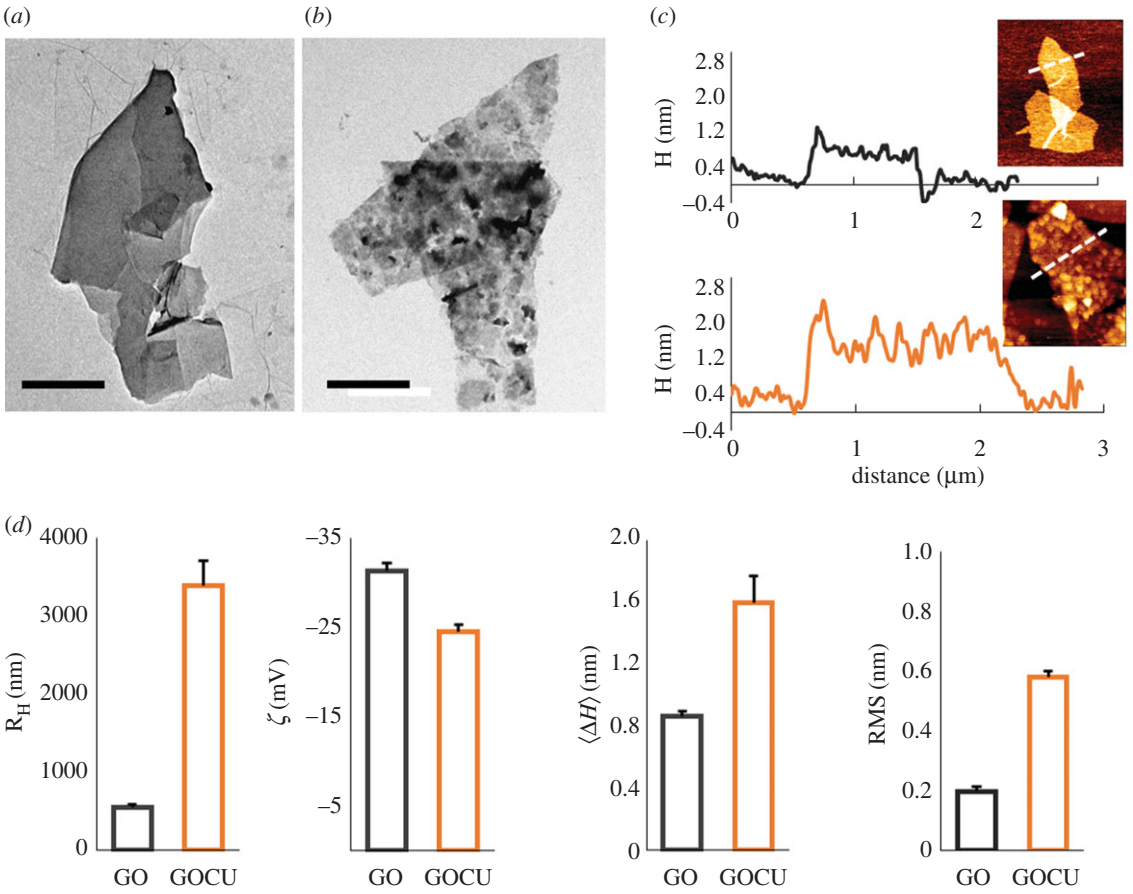

Figure 1. Characterization of GO and GOCU-2 representative TEM images of GO (*a*) and GOCU-2 (*b*) flakes, scale bar is 500 nm (*a*) and 1 µm (*b*). AFM height profiles of GO and GOCU surfaces (*c*), representative AFM height maps are shown in the insets. (*d*) Histograms of hydrodynamic radius, zeta potential, average height and RMS of GO and GOCU-2. (Online version in colour.)

From the measured curcumin concentration, we calculated the amount of GO surface covered by this compound as previously reported for lipid-covered GO [42]. The theoretical surface area of pristine graphene is 2630 $m^2\ g^{-1}$. Our GO contains approximately 45% of oxygen, so the maximal area available for molecule binding is 1.58 $m^2\ mg^{-1}$ if we consider both sides of the GO flakes [42]. However, because R_H measurements obtained by DLS show a multilayered structure of GOCU, GO sheets in solution are sandwiched between hydrophobic curcumins. For this reason, we consider only one side of the GO surface is available. The surface area of a curcumin molecule is 0.931 nm^2 and the final calculated adsorption on the GO surface goes from 28.9% (GOCU-1) to 88% (GOCU-3) (figure 2*d*). The GOCU stability over time was measured by optical density at 600 nm and is reported in figure 2*e*.

3.2. Antibacterial activity of graphene oxide and curcumin-conjugated graphene oxide

The loss of viability of MRSA was evaluated calculating the CFUs after exposure to GO or GOCU in water and by analysing MIC and MBC [43].

As shown in figure 3*a*, significant differences were found in MIC values of GO compared to GOCU. In the case of GO, there is no inhibition of the bacterial growth below 37.5 µg ml^{-1}. This result is in good agreement with other studies focused on GO activity on MRSA, where GO alone was not effective below 60 µg ml^{-1} [15,16].

In contrast, GOCU displays a significant inhibition of bacterial growth in a concentration-dependent manner. The MIC values obtained for GOCU-1, GOCU-2 and GOCU-3 are 2.8 µg ml^{-1}, 1.42 µg ml^{-1} and 1.06 µg ml^{-1} respectively (curcumin content) and 18.75 µg ml^{-1}, 4.7 µg ml^{-1} and 2.35 µg ml^{-1} respectively (GO content). Considering that the MIC of curcumin alone against MRSA ranges from 125 to 256 µg ml^{-1} [8], our results indicate a synergistic activity of GO and curcumin.

There have been several explanations on how curcumin kills the bacteria; the main hypothesis relies on the curcumin interaction with FtsZ (prokaryotic homologue of eukaryotic tubulin), and inhibition of protofilament formation and of bacterial cell proliferation. However, binding to peptidoglycan and perturbation of the bacterial membrane integrity have also been proposed as possible mechanisms [8].

As shown by zeta potential measurements, curcumin creates a corona around GO sheets that creates a less negative zeta potential, which makes GOCU more likely to bind to the negatively charged membrane of the *S. aureus* cells.

By analysing microscopy images, we can hypothesize a double action of GO and GOCU against MRSA membranes, resulting in disruption with debris visible after GOCU treatment (figure 3*e*). The GO alone seems to simply wrap MRSA cells, which appear intact, as in the control (figure 3*d* and figure 3*c*, respectively). This wrapping effect of GO has been already reported in the literature for several species [13] and can explain the high difference between MIC and MBC values observed for GO. The MBC/MIC ratio offers information

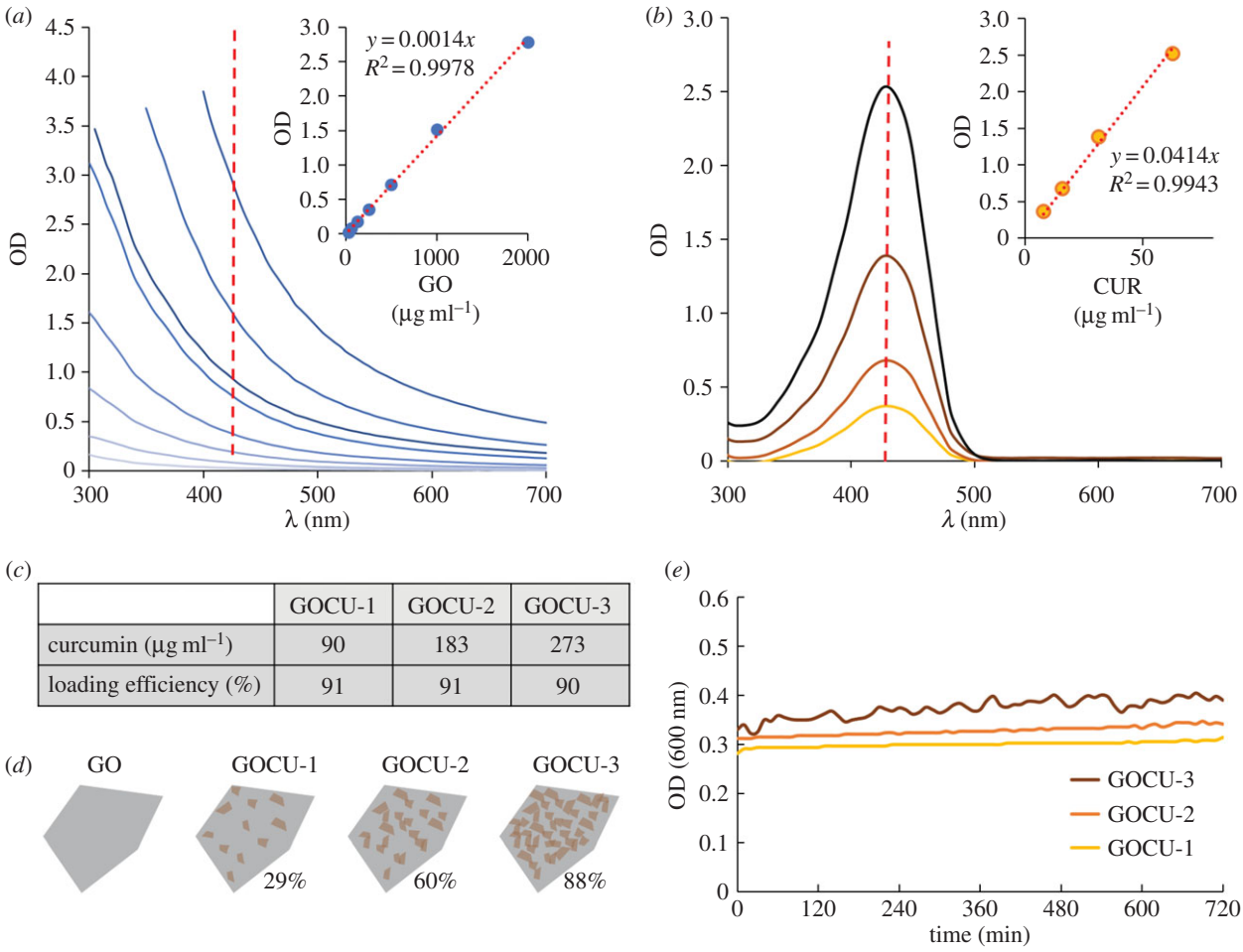

	GOCU-1	GOCU-2	GOCU-3
curcumin (μg ml^{-1})	90	183	273
loading efficiency (%)	91	91	90

Figure 2. Spectroscopic properties of GO and curcumin (*a–b*) and quantification of curcumin bound to GO in the GOCU composites and loading efficiency (*c*). (*d*) Illustration of curcumin loading in different samples (amount of surface covered by curcumin is indicated as a percentage). (*e*) GOCU stability in a 12 h period analysed by measuring OD at 600 nm. (Online version in colour.)

(*a*)

MIC (μg ml^{-1})

	GO	GOCU-1	GOCU-2	GOCU-3
GO	37.5	18.75	4.7	2.35
curcumin	--	2.8	1.42	1.06

MBC (μg ml^{-1})

GO	>150	18.75	7	2.35
curcumin	--	2.8	2.14	1.06

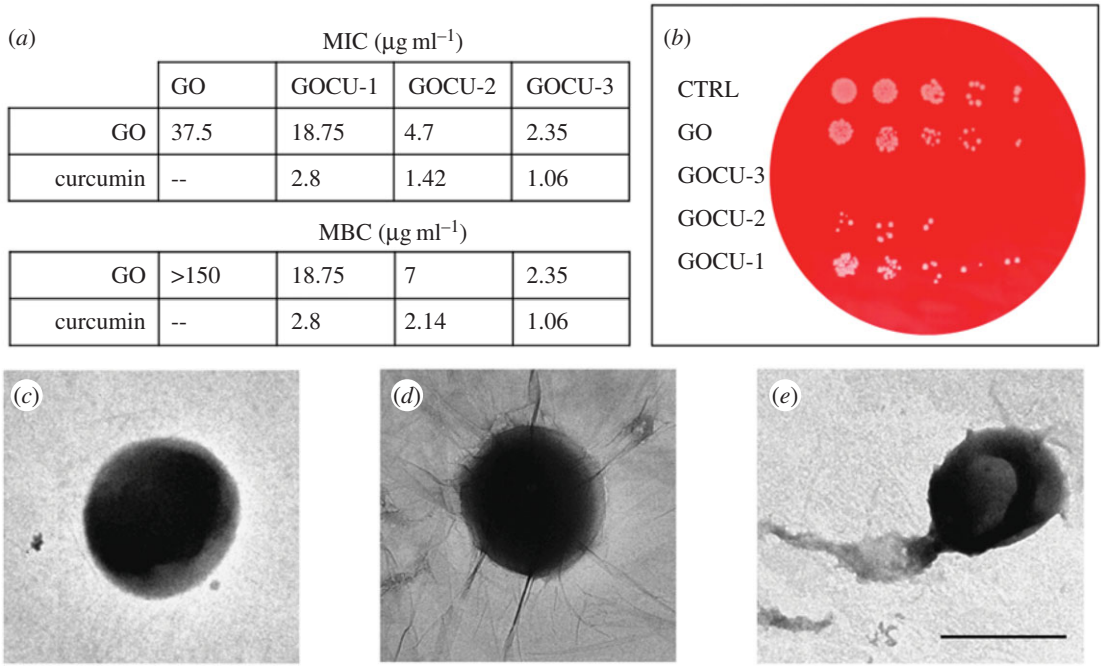

Figure 3. Antibacterial activity of GO and GOCU against MRSA (*a*) MIC and MBC values for each sample, GO and curcumin concentration measured are reported. (*b*) Exemplary plate obtained after treatment of MRSA with a GO concentration of 4.7 μg ml^{-1} in GO, GOCU-1, GOCU-2 and GOCU-3. TEM images of control (*c*), MRSA treated with GO (*d*) and MRSA treated with GOCU-2. (Online version in colour.)

about the nature of the antibacterial activity: if MBC/MIC is between 1 and 2, the drug is bactericidal, while if MBC/MIC is higher than 2, the antimicrobial substance can be classified as a bacteriostatic [16]. We therefore can conclude that while GOCU acts as a bactericidal of MRSA, GO alone is simply bacteriostatic through a wrapping-based mechanism.

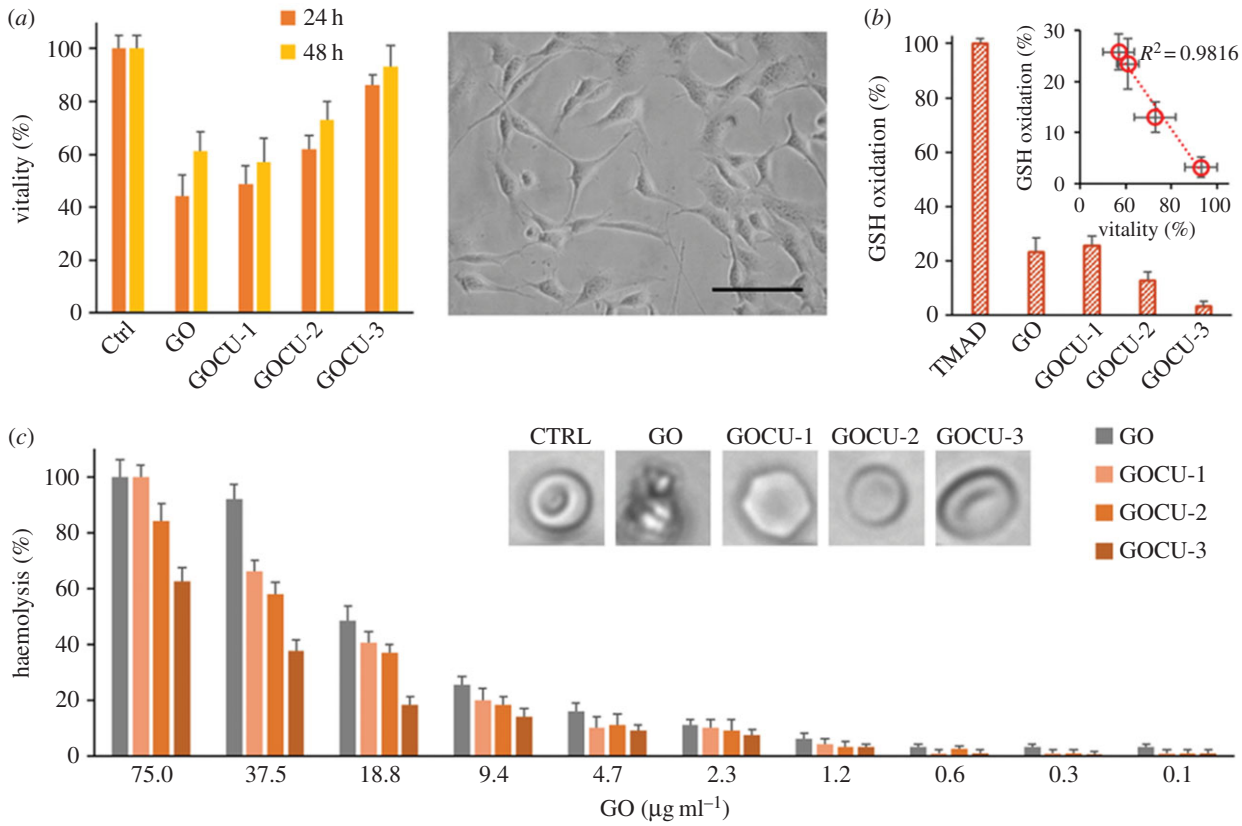

Figure 4. Vitality of 3T3 fibroblasts after administration of GO, GOCU-1, GOCU-2 and GOCU-3 with a concentration of GO of 50 μg ml^{-1} in each sample (*a*) and a representative image of cell morphology. (*b*) GSH oxidation mediated by GO, GOCU-1, GOCU-2 and GOCU-3 at 50 μg ml^{-1} compared to complete oxidation of GSH by diamide (TMAD). (*c*) Haemolytic activity of GO and GOCU at several concentrations normalized to 100% haemolysis of RBCs in ddH_2O. (Online version in colour.)

3.3. Cytotoxicity and oxidative stress mediated by graphene oxide and curcumin-conjugated graphene oxide

To examine the *in vitro* toxicity, we tested GO and GOCU at a fixed concentration of 50 μg ml^{-1} of GO on 3T3 fibroblasts and evaluated cell vitality after 24 or 48 h of exposure (figure 4*a*). Cell vitality is reduced by 50% in the presence of GO and GOCU-1, but is higher when GOCU-2 (approx. 70% of vitality after 48 h) or GOCU-3 (approx. 90% of vitality after 48 h) are administered, indicating that the increase in curcumin concentration decreases the GO-mediated cell mortality. Oxidative stress and generation of reactive oxygen species can be involved in the toxic effects of GO [44]. We evaluated the GSH oxidation mediated by different materials with a concentration of GO of 50 μg ml^{-1}, because GSH has a critical role in protecting cells from oxidative damage [45]. We observed that after administration of GO or GOCU-1, approx. 25% of the GSH is oxidized. This percentage is greatly reduced when curcumin concentration increases with approx. 13% of oxidation with GOCU-2 and approx. 3% of oxidation with GOCU-3. As shown in the inset in figure 4*b*, there is a linear relation between cell vitality and GSH oxidation. The presence of curcumin, a known radical scavenger and oxidation inhibitor, restores the reduced form of GSH and probably recovers the cell vitality. However, is also possible that the GO functionalization with curcumin limits the interaction of sharp GO edges with membranes: molecular dynamics simulations and bioimaging experiments revealed a direct bilayer penetration that begins with localized piercing at sharp corners or at protrusions along graphene edges as the mechanism of uptake of graphene sheets in mammalian cells [46]. The presence of curcumin in GOCU therefore could shield the edges of GO sheets and impede membrane puncturing. However, because the R_H of all GOCU tested is larger than that of GO sheets alone, the decrease in cytotoxicity with increase in curcumin concentration in each sample is more probably attributed to oxidation inhibition.

Following administration, the GO and GOCU nanomaterials may interact with blood components with a haemocompatibility determined by surface chemistry. It has been demonstrated that GO possesses a strong haemolytic activity that is reduced when a protein corona is absorbed on its surfaces due to the shielding of the extremely sharp edges of the GO sheets [27]. We quantified the haemolytic activity of GO and GOCU to test if the curcumin on the GO surface can avoid cutting of RBCs (figure 4*c*).

The incubation of GO samples with RBCs revealed a very high haemolytic activity of bare GO, as shown in the histogram of haemolysis in figure 4*c*. The GO has the highest haemolytic activity with over 90% haemolysis above 125 μg ml^{-1}, which decreases with decreasing concentration, from approximately 48% at 62.5 μg ml^{-1} to 25% at 31.25 μg ml^{-1}. With regard to the GOCU samples, haemolytic activity reduction is proportional to the curcumin loaded on graphene. At concentrations below 15 μg ml^{-1} the GO and GOCU samples caused a low haemolysis of approximately 10% without significant differences between samples.

In summary, as demonstrated by other studies on human serum and albumin, the corona adsorbed on a GO surface can markedly decrease haemolysis and enhance biocompatibility.

4. Conclusion

Multidrug resistance has widely increased worldwide and the most commonly used antibiotics became no longer effective in controlling infections. MRSA infections represent a global health challenge because the annual frequency of deaths from MRSA has rapidly increased and has surpassed deaths caused by human immunodeficiency virus/acquired immune deficiency syndrome [47]. A renewed interest on natural compounds like curcumin against MRSA has developed due to the high risk of side effects and development of resistance to conventional antibiotic therapies [8].

In this paper, we demonstrate the applicability of a composite based on curcumin-loaded graphene sheets (GOCU) as a highly effective antibacterial nanomaterial against MRSA. GOCU has a MIC of 1 $\mu g\ ml^{-1}$ (curcumin concentration) and the MBC/MIC ratio of GOCU indicates a definite bactericidal action compared to the bacteriostatic wrapping of GO alone [16]. The use of curcumin in synergistic activity with GO is a promising strategy to fight defences developed during millions of years of microbial evolution. On the one hand, GO possesses a high surface area and high efficiency of drug loading to deliver the poorly soluble curcumin against MRSA cells. On the other hand, the sharp GO edges, which would cause haemolytic effects, are shielded by curcumin molecules, reducing the cytotoxicity of this material. These features open new applications of GOCU in antibiotic-resistant infections treatment via the systemic route and for the development of antifouling surfaces for healthcare applications.

Data accessibility. This article has no additional data.

Authors' contributions. F.B., M.C., R.T., M.D.V. and M.S. carried out microbiological laboratory tests. V.P. and R.D.S. carried out the biophysical and microscopy experiments and data analysis, and drafted the manuscript; A.V. performed cytotoxicity experiments. C.C. carried out the statistical analyses. G.C. and M.D.S. revised the manuscript. M.P. designed and coordinated the study and helped draft the manuscript. All the authors gave their final approval for publication.

Competing interests. We declare we have no competing interests.

Funding. This research was funded by a Research Grant 2017 from the European Society of Clinical Microbiology and Infectious Diseases (ESCMID) to V.P.

Acknowledgements. Experiments have been performed at the LABCEMI Microscopy Facility (UCSC, Rome, Italy). We are extremely thankful to Mario Amici for the technical support during experiments.

References

1. Tenover FC. 2006 Mechanisms of antimicrobial resistance in bacteria. *Am. J. Med.* **119**, S3–S10. (doi:10.1016/j.amjmed.2006.03.011)
2. Kalan L, Wright GD. 2011 Antibiotic adjuvants: multicomponent anti-infective strategies. *Expert Rev. Mol. Med.* **13**, e5. (doi:10.1017/S1462399410001766)
3. Zouhir A, Jridi T, Nefzi A, Ben Hamida J, Sebei K. 2016 Inhibition of methicillin-resistant *Staphylococcus aureus* (MRSA) by antimicrobial peptides (AMPs) and plant essential oils. *Pharm. Biol.* **54**, 3136–3150. (doi:10.1080/13880209.2016.1190763)
4. Kennedy AD *et al.* 2008 Epidemic community-associated methicillin-resistant *Staphylococcus aureus*: recent clonal expansion and diversification. *Proc. Natl Acad. Sci. USA* **105**, 1327–1332. (doi:10.1073/pnas.0710217105)
5. Ray P, Gautam V, Singh R (eds). 2011 *Methicillin-resistant staphylococcus aureus (MRSA) in developing and developed countries: implications and solutions*. New Delhi, India: Regional Health Forum.
6. Bono VD, Giacobbe DR. 2016 Bloodstream infections in internal medicine. *Virulence* **7**, 353–365. (doi:10.1080/21505594.2016.1140296)
7. Padmanaban G, Rangarajan PN. 2016 Curcumin as an adjunct drug for infectious diseases. *Trends Pharmacol. Sci.* **37**, 1–3. (doi:10.1016/j.tips.2015.09.007)
8. Teow S-Y, Liew K, Ali SA, Khoo AS-B, Peh S-C. 2016 Antibacterial action of curcumin against *Staphylococcus aureus*: a brief review. *J. Trop. Med.* **2016**, 2853045.
9. Hussain Z, Thu HE, Ng S-F, Khan S, Katas H. 2017 Nanoencapsulation, an efficient and promising approach to maximize wound healing efficacy of curcumin: a review of new trends and state-of-the-art. *Colloids Surf B* **150**, 223–241. (doi:10.1016/j.colsurfb.2016.11.036)
10. Feng L, Zhang S, Liu Z. 2011 Graphene based gene transfection. *Nanoscale* **3**, 1252–1257. (doi:10.1039/c0nr00680g)
11. Palmieri V, Papi M, Conti C, Ciasca G, Maulucci G, De Spirito M. 2016 The future development of bacteria fighting medical devices: the role of graphene oxide. *Expert Rev. Med. Devices* **13**, 1013–1019. (doi:10.1080/17434440.2016.1245612)
12. Papi M *et al.* 2016 Biomimetic antimicrobial cloak by graphene-oxide agar hydrogel. *Sci. Rep.* **6**, 12. (doi:10.1038/s41598-016-0010-7)
13. Palmieri V, Lauriola MC, Ciasca G, Conti C, De Spirito M, Papi M. 2017 The graphene oxide contradictory effects against human pathogens. *Nanotechnology* **28**, 152001. (doi:10.1088/1361-6528/aa6150)
14. Palmieri V *et al.* 2017 Bacteria meet graphene: modulation of graphene oxide nano-sheets interaction with human pathogens for an effective antimicrobial therapy. *ACS Biomat. Sci. Eng.* **3**, 619–627. (doi:10.1021/acsbiomaterials.6b00812)
15. Marta B, Potara M, Iliut M, Jakab E, Radu T, Imre-Lucaci F, Katona G, Popescu O, Astilean S. 2015 Designing chitosan–silver nanoparticles–graphene oxide nanohybrids with enhanced antibacterial activity against *Staphylococcus aureus*. *Colloids Surf. A* **487**, 113–120. (doi:10.1016/j.colsurfa.2015.09.046)
16. de Moraes ACM, Lima BA, de Faria AF, Brocchi M, Alves OL. 2015 Graphene oxide-silver nanocomposite as a promising biocidal agent against methicillin-resistant *Staphylococcus aureus*. *Int. J. Nanomedicine* **10**, 6847–6861. (doi:10.2147/IJN.S90660)
17. Pan W-Y, Huang C-C, Lin T-T, Hu H-Y, Lin W-C, Li M-J, Sung H-W. 2016 Synergistic antibacterial effects of localized heat and oxidative stress caused by hydroxyl radicals mediated by graphene/iron oxide-based nanocomposites. *Nanomedicine* **12**, 431–438. (doi:10.1016/j.nano.2015.11.014)
18. Ristic BZ *et al.* 2014 Photodynamic antibacterial effect of graphene quantum dots. *Biomaterials* **35**, 4428–4435. (doi:10.1016/j.biomaterials.2014.02.014)
19. Zhang B, Wei P, Zhou Z, Wei T. 2016 Interactions of graphene with mammalian cells: molecular mechanisms and biomedical insights. *Adv. Drug Deliv. Rev.* **105**, 145–162. (doi:10.1016/j.addr.2016.08.009)
20. Hatamie S, Akhavan O, Sadrnezhaad SK, Ahadian MM, Shirolkar MM, Wang HQ. 2015 Curcumin-reduced graphene oxide sheets and their effects on human breast cancer cells. *Mater. Sci. Eng. C* **55**, 482–489. (doi:10.1016/j.msec.2015.05.077)
21. Maity AR, Chakraborty A, Mondal A, Jana NR. 2014 Carbohydrate coated, folate functionalized colloidal graphene as a nanocarrier for both hydrophobic and hydrophilic drugs. *Nanoscale* **6**, 2752–2758. (doi:10.1039/c3nr05431d)
22. Some S *et al.* 2014 Cancer therapy using ultrahigh hydrophobic drug-loaded graphene derivatives. *Sci. Rep.* **4**, 6314. (doi:10.1038/srep06314)
23. Muthoosamy K, Abubakar IB, Bai RG, Loh H-S, Manickam S. 2016 Exceedingly higher co-loading of curcumin and paclitaxel onto polymer-functionalized reduced graphene oxide for highly potent synergistic anticancer treatment. *Sci. Rep.* **6**, 32808. (doi:10.1038/srep32808)
24. Barua S, Chattopadhyay P, Phukan MM, Konwar BK, Islam J, Karak N. 2014 Biocompatible

hyperbranched epoxy/silver–reduced graphene oxide–curcumin nanocomposite as an advanced antimicrobial material. *RSC Adv.* **4**, 47 797–47 805. (doi:10.1039/C4RA07802K)

25. Drake PL, Hazelwood KJ. 2005 Exposure-related health effects of silver and silver compounds: a review. *Ann. Occup. Hyg.* **49**, 575–585.
26. Silver S. 2003 Bacterial silver resistance: molecular biology and uses and misuses of silver compounds. *FEMS Microbiol. Rev.* **27**, 341–353. (doi:10.1016/S0168-6445(03)00047-0)
27. Papi M, Lauriola M, Palmieri V, Ciasca G, Maulucci G, De Spirito M. 2015 Plasma protein corona reduces the haemolytic activity of graphene oxide nano and micro flakes. *RSC Adv.* **5**, 81 638–81 641. (doi:10.1039/C5RA15083C)
28. Papi M, Palmieri V, Maulucci G, Arcovito G, Greco E, Quintiliani G, Fraziano M, De Spirito M. 2011 Controlled self assembly of collagen nanoparticle. *J. Nanopart. Res.* **13**, 6141–6147. (doi:10.1007/s11051-011-0327-x)
29. Maiorana A *et al.* 2015 Effect of alginate lyase on biofilm-grown Helicobacter pylori probed by atomic force microscopy. *Int. J. Polymer Sci.* **2015**, 989516. (doi:10.1155/2015/989516)
30. Palmieri V, Lucchetti D, Maiorana A, Papi M, Maulucci G, Ciasca G, Svelto M, De Spirito M, Sgambato A. 2014 Biomechanical investigation of colorectal cancer cells. *Appl. Phys. Lett.* **105**, 123701. (doi:10.1063/1.4896161)
31. Torelli R *et al.* 2017 Different effects of matrix degrading enzymes towards biofilms formed by *E. faecalis* and *E. faecium* clinical isolates. *Colloids Surf B.* **158**, 349–355. (doi:10.1016/j.colsurfb.2017.07.010)
32. Palmieri V *et al.* 2014 Dynamic light scattering for the characterization and counting of extracellular vesicles: a powerful noninvasive tool. *J. Nanopart. Res.* **16**, 2583. (doi:10.1007/s11051-014-2583-z)
33. Perreault F, De Faria AF, Nejati S, Elimelech M. 2015 Antimicrobial properties of graphene oxide nanosheets: why size matters. *ACS Nano* **9**, 7226–7236. (doi:10.1021/acsnano.5b02067)
34. Kosower NS, Kosower EM, Wertheim B, Correa WS. 1969 Diamide, a new reagent for the intracellular oxidation of glutathione to the disulfide. *Biochem. Biophys. Res. Commun.* **37**, 593–596. (doi:10.1016/0006-291X(69)90850-X)
35. Su Q, Pang S, Alijani V, Li C, Feng X, Müllen K. 2009 Composites of graphene with large aromatic molecules. *Adv. Mater.* **21**, 3191–3195. (doi:10.1002/adma.200803808)
36. Akhavan O, Ghaderi E, Abouei E, Hatamie S, Ghasemi E. 2014 Accelerated differentiation of neural stem cells into neurons on ginseng-reduced graphene oxide sheets. *Carbon* **66**, 395–406. (doi:10.1016/j.carbon.2013.09.015)
37. Gao J, Liu F, Liu Y, Ma N, Wang Z, Zhang X. 2010 Environment-friendly method to produce graphene that employs vitamin C and amino acid. *Chem. Mater.* **22**, 2213–2218. (doi:10.1021/cm902635j)
38. Esfandiar A, Akhavan O, Irajizad A. 2011 Melatonin as a powerful bio-antioxidant for reduction of graphene oxide. *J. Mater. Chem.* **21**, 10 907–10 914. (doi:10.1039/c1jm10151j)
39. Akhavan O, Kalaee M, Alavi Z, Ghiasi S, Esfandiar A. 2012 Increasing the antioxidant activity of green tea polyphenols in the presence of iron for the reduction of graphene oxide. *Carbon* **50**, 3015–3025. (doi:10.1016/j.carbon.2012.02.087)
40. Yang XX, Li CM, Li YF, Wang J, Huang CZ. 2017 Synergistic antiviral effect of curcumin functionalized graphene oxide against respiratory syncytial virus infection. *Nanoscale* **9**, 16 086–16 092. (doi:10.1039/C7NR06520E)
41. Patra D, Barakat C. 2011 Synchronous fluorescence spectroscopic study of solvatochromic curcumin dye. *Spectrochim. Acta, Part A* **79**, 1034–1041. (doi:10.1016/j.saa.2011.04.016)
42. Huang P-JJ, Wang F, Liu J. 2016 Liposome/graphene oxide interaction studied by isothermal titration calorimetry. *Langmuir* **32**, 2458–2463. (doi:10.1021/acs.langmuir.6b00006)
43. Hazan R, Que Y-A, Maura D, Rahme LG. 2012 A method for high throughput determination of viable bacteria cell counts in 96-well plates. *BMC Microbiol.* **12**, 259. (doi:10.1186/1471-2180-12-259)
44. Jarosz A, Skoda M, Dudek I, Szukiewicz D. 2015 Oxidative stress and mitochondrial activation as the main mechanisms underlying graphene toxicity against human cancer cells. *Oxid. Med. Cell. Longev.* **2016**, 5851035.
45. Forman HJ, Zhang H, Rinna A. 2009 Glutathione: overview of its protective roles, measurement, and biosynthesis. *Mol. Aspects Med.* **30**, 1–12. (doi:10.1016/j.mam.2008.08.006)
46. Li Y, Yuan H, von dem Bussche A, Creighton M, Hurt RH, Kane AB, Gao H. 2013 Graphene microsheets enter cells through spontaneous membrane penetration at edge asperities and corner sites. *Proc. Natl Acad. Sci. USA* **110**, 12 295–12 300. (doi:10.1073/pnas.1222276110)
47. Bancroft EA. 2007 Antimicrobial resistance: it's not just for hospitals. *JAMA* **298**, 1803–1804. (doi:10.1001/jama.298.15.1803)